Magnetic dipole excitations of ^{50}Cr

H. Pai,[1,*] T. Beck,[1] J. Beller,[1] R. Beyer,[2] M. Bhike,[3,4] V. Derya,[5] U. Gayer,[1] J. Isaak,[6,7] Krishichayan,[3,4] J. Kvasil,[8] B. Löher,[1,6] V. O. Nesterenko,[9] N. Pietralla,[1] G. Martínez-Pinedo,[1,10] L. Mertes,[1] V. Yu. Ponomarev,[1] P.-G. Reinhard,[11] A. Repko,[8] P. C. Ries,[1] C. Romig,[1] D. Savran,[6,7] R. Schwengner,[2] W. Tornow,[3,4] V. Werner,[1] J. Wilhelmy,[5] A. Zilges,[5] and M. Zweidinger[1]

[1]*Institut für Kernphysik, Technische Universität Darmstadt, D-64289 Darmstadt, Germany*
[2]*Institut für Strahlenphysik, Helmholtz-Zentrum Dresden-Rossendorf, D-01328 Dresden, Germany*
[3]*Department of Physics, Duke University, Durham, North Carolina 27708, USA*
[4]*Triangle Universities Nuclear Laboratory, Durham, North Carolina 27708, USA*
[5]*Institut für Kernphysik, Universität zu Köln, D-50937 Köln, Germany*
[6]*ExtreMe Matter Institute EMMI and Research Division, GSI Helmholtzzentrum für Schwerionenforschung GmbH, D-64291 Darmstadt, Germany*
[7]*Frankfurt Institute for Advanced Studies FIAS, D-60438 Frankfurt am Main, Germany*
[8]*Institute of Particle and Nuclear Physics, Charles University, CZ-18000, Prague 8, Czech Republic*
[9]*Laboratory of Theoretical Physics, Joint Institute for Nuclear Research, Dubna, Moscow region, 141980, Russia*
[10]*GSI Helmholtzzentrum für Schwerionenforschung, Planckstraße 1, D-64291 Darmstadt, Germany*
[11]*Institut für Theoretische Physik II, Universität Erlangen, D-91058, Erlangen, Germany*

The low-lying $M1$ strength of the open-shell nucleus ^{50}Cr has been studied with the method of nuclear resonance fluorescence up to 9.7 MeV using bremsstrahlung at the superconducting Darmstadt linear electron accelerator S-DALINAC and Compton backscattered photons at the High Intensity γ-ray Source (HIγS) facility between 6 and 9.7 MeV of the initial photon energy. Fifteen 1^+ states have been observed between 3.6 and 9.7 MeV. Following our analysis the lowest 1^+ state at 3.6 MeV can be considered as an isovector orbital mode with some spin admixture. The obtained results generally match the estimations and trends typical for the scissors-like mode. Detailed calculations within the Skyrme quasiparticle random-phase-approximation method and the large-scale shell model justify our conclusions. The calculated distributions of the orbital current for the lowest 1^+-state suggest the schematic view of Lipparini and Stringari (isovector rotation-like oscillations inside the rigid surface) rather than the scissors-like picture of Lo Iudice and Palumbo. The spin $M1$ resonance is shown to be mainly generated by spin-flip transitions between the orbitals of the fp shell.

I. INTRODUCTION

During the last decades, investigation of strong magnetic dipole ($M1$) transitions in medium-mass nuclei was of a keen interest [1–6]. First of all, this was caused by a diversity of various physical effects related to these excitations: quenching of spin strength and impact of non-nucleonic degrees of freedom, relation to Gamow-Teller transitions and relevant astrophysical problems, isospin degrees of freedom of valence-shell excitations, peculiarities of the orbital scissors-like mode, cross-shell and l-forbidden transitions, impact of complex configurations, etc. Furthermore, these nuclei are accessible to modern large-scale shell model calculations [7,8] that have the capability to describe the effects mentioned above. Theoretical efforts and advanced experiments have finally led to a significant progress in understanding the features of $M1$ excitations in this mass region [6].

Open-shell fp-shell nuclei are particularly important in this activity [9–11]. Description of these nuclei is rather complicated because here deformation and pairing effects come to play. At the same time, these effects make the physics of fp-shell nuclei much richer. In particular, deformation results in the appearance of the low-energy orbital scissors-like $M1$ mode ($1^+_{\rm sc}$) [13–16].

So far the experimental data on the $M1$ $1^+_{\rm sc}$ strength in the fp region were limited to a few axially deformed nuclei: ^{46,48}Ti ($Z = 22$) [1] and ^{56}Fe ($Z = 26$) [9]. It was found that the $1^+_{\rm sc}$ in these nuclei is mainly represented by one low-energy (in the region 3.4–4.4 MeV) state with $K^\pi = 1^+$. As expected [13–16], this state is characterized by a strong $M1$ transition to the ground state. The theoretical analysis [1,9,12] indicates that the $1^+_{\rm sc}$ in this mass region is of a mixed (orbital + spin) character, although with a dominant orbital contribution. Shell-model calculations [9] demonstrate a considerable dependence of the description on a subtle balance of different effects such as equilibrium deformation, pairing, interaction parameters, etc.

For a better understanding of the $1^+_{\rm sc}$ features in fp-shell nuclei, we certainly need experimental data for deformed Cr ($Z = 24$) isotopes placed between the Ti and Fe chains. $J^\pi = 1^+$ states of ^{50}Cr are known from previous (p,p') experiments [17] and for three of them γ-ray transitions have been measured in nuclear resonance fluorescence (NRF) [18,19]. $B(M1)$ values are known only for two 1^+ states of ^{50}Cr. A comprehensive $M1$ strength distribution is missing. It is the purpose of the present study to provide data for a more comprehensive $M1$ strength distribution for the deformed nucleus ^{50}Cr.

*hari.vecc@gmail.com, hpai@ikp.tu-darmstadt.de

This nucleus was studied in photon scattering experiments using NRF [20–22]. The experiment was performed at the superconducting Darmstadt electron linear accelerator S-DALINAC [23] using unpolarized bremsstrahlung with a continuous spectral distribution from the Darmstadt High Intensity Photon Setup (DHIPS) [24]. Parity quantum numbers of spin-1 states were determined using the High Intensity γ-Ray Source [25] operated by the Triangle Universities Nuclear Laboratory and the Duke Free Electron Laser Laboratory (DFELL) at Duke University in Durham, NC, USA.

In the present experiment, the spectrum of ^{50}Cr up to 9.7 MeV and the corresponding $M1$ strength were determined. The $M1$ strength for the lowest $K^\pi = 1^+$ state with excitation energy of 3628.2 keV was obtained and the $B(M1)$ values for 12 strongly excited 1^+ states were measured for the first time.

Two theoretical models were used for further interpretation: Skyrme quasiparticle random-phase approximation (QRPA) [26,27] and large-scale shell model (LSSM) [8]. The self-consistent QRPA and LSSM rather well reproduce the experimental axial quadrupole deformation $\beta_{\mathrm{exp}} = 0.2897(44)$ [28] of ^{50}Cr and provided qualitatively close results. The calculations agree upon the feature that the 3628.2-keV state has predominantly orbital character with a minor spin admixture. This means that the present experiment provides observation of the 1^+_{sc} in Cr isotopes. The new data essentially supplement the 1^+_{sc} systematics in fp-shell nuclei and, as shown below, lead to a better understanding of 1^+_{sc} features in this mass region. Besides our analysis of the orbital flow implies a closer correspondence to the schematic view of Lipparini and Stringari [29] corresponding to isovector rotation-like oscillations of the nucleons inside the rigid nuclear surface than to the scissors-like picture of Lo Iudice and Palumbo [13].

The paper is organized as follows. In Sec. II, the experimental method and data analysis are outlined. In Sec. III, the theoretical analysis of the results is given. Sec. IV provides a summary.

II. EXPERIMENTAL METHOD AND DATA ANALYSIS

In NRF measurements, the excitation mechanism is purely electromagnetic. Therefore, intrinsic properties like spin, parity, and transition probabilities can be determined from the measured quantities (angular distribution, polarization asymmetries, γ-ray energy, and intensity [20–22]) in a model-independent way. For details of the NRF method, basic relations between the detected number of events and energy-integrated cross sections, transition widths as well as $M1$ transition strengths, we refer the reader to the reviews by Metzger [22] and Kneissl and coworkers [20,21]. Spin quantum numbers, cross sections $I_{i,0}$ (energy-integrated scattering cross sections for exciting a state i and de-exciting this state to the ground state 0), ground-state transition widths Γ_0, and transition strengths $B(M1)$ were measured at the DHIPS setup.

A series of NRF experiments was performed at TU Darmstadt and at Duke University. The photon-scattering experiment with unpolarized bremsstrahlung from the Darmstadt linear electron accelerator S-DALINAC [23] was performed at the Darmstadt High Intensity Photon Setup (DHIPS) [24]. Two measurements on ^{50}Cr were performed with bremsstrahlung at

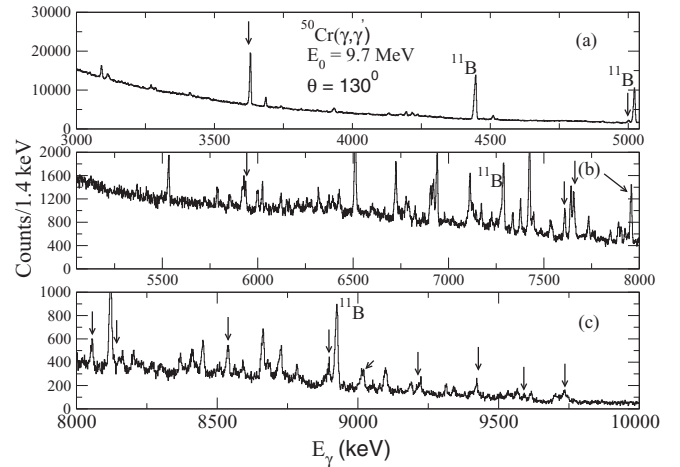FIG. 1. Photon scattering spectra of the ^{50}Cr(γ,γ') reaction from DHIPS between 3000 keV and 10000 keV for the 130° detector, measured at $E_0 = 9.7$ MeV. Ground-state $M1$ transitions of ^{50}Cr are indicated by arrows.

endpoint energies of 7.5(1) MeV and 9.7(1) MeV, respectively. The measurement with 7.5(1) MeV bremsstrahlung has been carried out to identify transitions via intermediate states. Bremsstrahlung has been produced by completely stopping the intense electron beam from the S-DALINAC's injector in a thick copper radiator target. The generated photon beam passes a massive copper collimator resulting in a beam spot with a size of about 2.5 cm diameter at the NRF target position. Target nuclei are excited by the resonant absorption of photons and subsequently decay either directly or via intermediate states to the ground state.

Scattered γ rays were detected by three HPGe detectors with 100% efficiency relative to a standard 3 in. × 3 in. NaI detector at a γ-ray energy of 1.3 MeV. They are placed at polar angles of 90° and 130° with respect to the incident beam. The detectors were surrounded by lead and BGO Compton suppression shields. The first measurement was performed with 2.0 g of an isotopically enriched ^{50}Cr target (96.416% enriched) using an end-point energy of $E_0 = 9.7(1)$ MeV and average electron beam currents of about 20 μA. In this measurement data were taken for about 131 h. For energy and photon-flux calibrations 399.3 mg of enriched ^{11}B (99.52% enriched) were used that were irradiated simultaneously. The efficiency of the two HPGe detectors was determined with a ^{56}Co source up to about 3500 keV energy. For higher photon energies the gamma-ray detection efficiencies were extracted from a simulation using the GEANT4 toolkit [30]. The second measurement was performed with the same target mass using an end-point energy at $E_0 = 7.5(1)$ MeV and average electron beam currents of about 33 μA. In this measurement, data were taken for about 105 h.

Photon scattering spectra of the ^{50}Cr(γ,γ') reaction from DHIPS between 3000 and 10000 keV for the detector at 130°, measured at $E_0 = 9.7(1)$ MeV are shown in Fig. 1. We have observed 33 excited states of ^{50}Cr with spin quantum numbers $J = 1$. In this work, we focus on $J^\pi = 1^+$ states. $M1$ transitions to the ground state of ^{50}Cr are indicated in
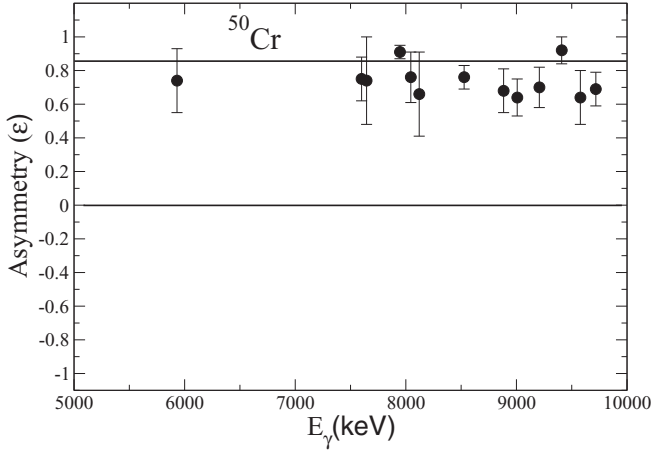
FIG. 2. Experimental asymmetry for the $M1$ transitions observed at HIγS.

Fig. 1 by arrows. In the following, transitions corresponding to direct decays to the ground state are called elastic transitions and those decaying via intermediate states will be referred to as inelastic transitions.

Parity quantum numbers of spin-1 states were determined at the High Intensity γ-Ray Source [25] operated by the Triangle Universities Nuclear Laboratory and the Duke Free Electron Laser Laboratory (DFELL) at Duke University in Durham, NC, USA. This facility provides a quasi-monoenergetic beam of nearly completely linearly polarized photons from laser Compton backscattering (LCB) in the entrance channel. For details of the analysis procedure, we refer the reader to Refs. [31,32]. The measurement was performed with 2.0 g of an isotopically enriched ^{50}Cr target (96.416% enriched). The target was centered between four HPGe detectors which were placed in a cross-like geometry at polar angles of $90°$ with respect to the incident beam, two of them have 100% relative efficiency and the other two have 60% relative efficiency, respectively. In this setup, two detectors were placed in the (horizontal) polarization plane of the incident γ-ray beam at azimuthal angles $\varphi = 0°$ and $\varphi = 180°$ and the other two were placed perpendicular to it at $\varphi = 90°$ and $\varphi = 270°$, respectively.

The experimental asymmetries ε for the $M1$ transitions observed in the measurements at HIγS are shown in Fig. 2. The asymmetry ε is defined by the ratio of the measured and efficiency-corrected peak intensities $A_\parallel$ and $A_\perp$, within and perpendicular to the polarization plane, respectively:

$$\varepsilon = \frac{A_\parallel - A_\perp}{A_\parallel + A_\perp} = q\Sigma. \tag{1}$$

Here, Σ is the analyzing power and q is the experimental sensitivity which accounts for the finite opening angles of the detectors and the finite size of the target. The analyzing power Σ of NRF amounts to $+1$ for a $J^\pi = 1^+$ state and -1 for $J^\pi = 1^-$ state, respectively. For this setup, the experimental sensitivity q amounts to 0.86(1). In total 13 $M1$ excitations of ^{50}Cr have been observed in this experiment.

III. RESULTS AND DISCUSSION

A. Experimental results

The experimental results are summarized in Table I and Fig. 3. In the present work, we have deduced $M1$ strengths in ^{50}Cr for the first time through the (γ, γ') reaction in addition to the 3628.0-keV transition, whose $M1$ strength has previously been measured via (γ, γ') [18] and (e, e') [1,17,33] experiments albeit with larger uncertainties. In the present experiment, the uncertainty of the cross section has been reduced for the 3628.0-keV transition. Nine of the observed excited states of ^{50}Cr may be already known from a (p, p') experiment [17] and three states (3628.2, 7645.7, and 8885.6 keV) were known from (γ, γ') [18,19] experiments. For 12 1^+ states of ^{50}Cr, our data provide first information on their γ-decay transitions.

Using linearly polarized quasi-monoenergetic photons at HIγS, positive parity quantum numbers were assigned to 13 states apart from the 3628.2-keV state. The definite positive parity quantum number assignment for the 3628.2-keV state has been adopted from earlier (p, p') and (e, e') [1,17,33] experiments. Three new $M1$ transitions (5930.8, 8045.1, and 8120.8 keV) have been identified in the present work and for 13 1^+ states $M1$ excitation strengths have been obtained for the first time.

The experimental $B(M1)$ values into the ground state are shown in Fig. 3. The $M1$ strength distribution exhibits an intriguing pattern: an isolated, rather strong $M1$ excitation at low energy at 3.6 MeV is separated from an accumulation of fragmented $M1$ strength above 7 MeV. A strongly excited $J^\pi = 1^+$ state at an excitation energy of 3628.2 keV with a strength of $B(M1)\uparrow = 1.113(49)$ μ_N^2 is observed. The rest of the observed $M1$ excitations in ^{50}Cr is expected [17] to be generated by spin excitations, mainly from $f_{7/2} \rightarrow f_{5/2}$ orbitals like in ^{52}Cr [35]. We will first concentrate on the 1^+ state at 3628.2 keV. This state could correspond to a moderately collective scissors-like mode. This mode has been predicted [13,14] and then discovered in (e, e') reactions by Richter *et al.* [15] in heavy deformed nuclei. As mentioned above, the 1_{sc}^+ state was also reported in the open fp shell nuclei ^{46}Ti, ^{48}Ti [1], and ^{56}Fe $(Z = 26)$ [9].

The experimental value of the quadrupole deformation parameter β_{exp} for ^{50}Cr is 0.2897(44) [28], which indicates that this nucleus is well deformed and hence can support the formation of a 1_{sc}^+ state. The ratio of the $M1$ transition rates of the 1^+ level at 3628.2 keV to the ground state and the first-excited 2^+ state (at 783.32 keV excitation energy) is found to be $\frac{B(M1;1_1^+ \rightarrow 2_1^+)}{B(M1;1_1^+ \rightarrow 0_1^+)} = \frac{\Gamma_\perp}{\Gamma_0}(\frac{E_{\gamma 0}}{E_{\gamma 1}})^3 = 1.02(2)$ with $E_{\gamma 0,(1)}$ being the γ-ray transition energy to the ground (first-excited) state. This value is larger by a factor of 2 compared to the value of 0.5 obtained by employing the Alaga rule [36]. This discrepancy hints at some degree of K mixing, perhaps ^{50}Cr exhibits some degree of γ softness [37].

Since in ^{50}Cr neutron and proton Fermi levels are in the same open subshell, spin magnetism is also expected in the lowest 1^+ state. Therefore, the state at 3628.2 keV should be of a mixed orbital/spin nature. It is also excited in (p, p') reactions [17], which points to a sufficient contribution of spin-$M1$ strength.

TABLE I. Transitions observed in the ^{50}Cr(γ,γ') reaction with an endpoint energy of 9.7 MeV. Experimental uncertainties of the excitation energies are less then 0.5 keV.

E_x [a] (keV)	E_γ [a] (keV)	$\frac{W(90°)}{W(130°)}$	J^π	$I_{i,0}$ (eVb)	Γ_0 (eV)	$\frac{\Gamma_i}{\Gamma_0}$ [b]	$B(M1)\uparrow$ (μ_N^2)	$B(M1)\uparrow$ (μ_N^2)	Γ_0^{red} (meV/MeV^3)
3628.2	3628.0	0.74(2)	$1^{+\text{c}}$	120(5)	0.205(9)		1.113(49)	0.99(12)[d]	4.29(19)
	2845.0					0.49(1)			
4997.0	4996.7	0.78(6)	$1^{(+)\text{e}}$	16.2(12)	0.070(7)		0.145(15)	–	0.56(6)
	4213.8					1.0(1)			
5931.2	5930.8	0.92(9)	1^+	23.9(20)	0.073(6)	–	0.091(7)	–	0.35(3)
7600.8	7600.2	0.80(10)	1^+	66.4(73)	0.334(37)	–	0.197(22)	–	0.76(8)
7645.7	7645.1	0.69(17)	1^+	23.2(28)	0.118(14)	–	0.068(8)	–	0.26(3)
7948.1	7947.4	0.78(3)	1^+	197.7(96)	1.382(79)		0.714(41)	–	2.75(16)
	7164.5					0.27(2)			
8045.8	8045.1	0.77(10)	1^+	42.2(47)	0.238(26)	–	0.118(13)	–	0.46(5)
8121.5	8120.8	0.76(20)	1^+	16.4(20)	0.094(11)	–	0.045(5)	–	0.18(2)
8528.1	8527.4	0.70(8)	1^+	96(11)	0.85(11)		0.353(48)	–	1.36(18)
	7743.1					0.39(6)			
8885.6	8884.8	0.82(8)	1^+	77.7(68)	0.534(47)	–	0.197(17)	0.277(74)[e]	0.76(7)
9007.9	9007.0	0.88(13)	1^+	40.5(48)	0.286(34)	–	0.101(12)	–	0.39(5)
9208.3	9207.4	0.77(20)	1^+	50(12)	0.369(89)	–	0.123(30)	–	0.47(11)
9409.5	9408.5	0.78(14)	1^+	105(17)	0.81(13)	–	0.252(41)	–	0.97(16)
9579.1	9578.1	0.97(25)	1^+	37.7(78)	0.301(62)	–	0.089(18)	–	0.34(7)
9719.1	9718.1	0.85(11)	1^+	173(21)	1.42(17)	–	0.402(49)	–	1.55(19)

[a]The difference between the the excitation energy (E_x) and transition energy [γ-ray energy (E_γ)] is due to the nuclear recoil.
[b]Branching ratio.
[c]From Refs. [1,17,33].
[d]From Ref. [18].
[e]From Ref. [34].

The available experimental results for the 1^+_{sc} in fp-shell nuclei, including the present data, are exhibited in Fig. 4. It is instructive to see how much these data match early [2,6,16,38]

$$E = 66\delta A^{-1/3} \text{ MeV}, \qquad (2)$$

$$B(M1) = 0.0042 E A^{5/3} \delta^2 g_r^2 \ \mu_N^2, \qquad (3)$$

and modified [39]

$$E = 13.4\sqrt{1 + (3\delta)^2} A^{-1/3} \text{ MeV}, \qquad (4)$$

$$B(M1) = 0.66 \frac{\delta^3}{1 + (3\delta)^2} A^{4/3} g_{\text{eff}}^2 \ \mu_N^2, \qquad (5)$$

empirical estimations for 1^+_{sc} energies and $B(M1)$ values. Here, $\delta = 0.946\beta$ is the deformation parameter; $g_r = 2Z/A$ is the
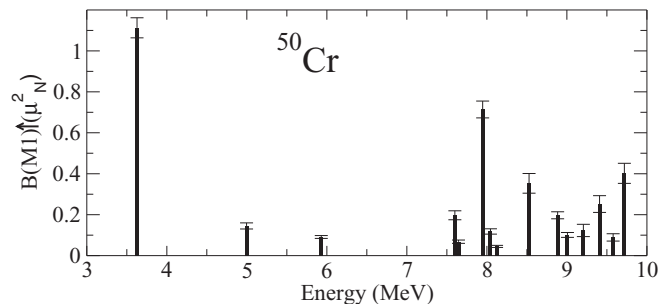
orbital factor, $g_{\text{eff}} = c_g g_r$ with $c_g = 0.8$ [39]. The deformation parameter β in Figs. 4–7 is related to the value $B(E2)\uparrow = B(E2, 0^+_1 \rightarrow 2^+_1)$ as [40] $\beta_{\exp} = \frac{4\pi}{3ZR_0^2}\sqrt{B(E2)\uparrow/e^2}$ with $R_0 = 1.2 \ A^{1/3}$fm. As seen below from Fig. 5, estimations (2)–(3) and (4)–(5) give for fp-shell nuclei rather close results.

The data are compared to the estimates according to Eqs. (2)–(3) and (4)–(5) in Fig. 5. We see in panel (a) that the experimental values lie somewhat below the estimation but closely follow the linear dependence on the deformation parameter, which is a strong fingerprint of a scissors-like excitation. Our data on ^{50}Cr well fit this trend. Following panel (b), the correspondence of the experimental and estimated $B(M1)$ values is also quite satisfactory. Some deviations from the phenomenological estimates can be explained by that in fp nuclei the states are determined by a few two quasiparticle (2qp) components and the orbital motion is supplemented by a significant spin admixture (see discussion below). Altogether one may state that our results for the state at 3.628 MeV rather well fit the 1^+_{sc} systematics, which justifies the assignment of predominantly scissors-like nature to this state. In the next section, our theoretical analysis presents additional arguments in favor of this conclusion.

FIG. 3. The experimental $B(M1)$ values for the ground state transitions.

B. Theoretical analysis

The $M1$ strength in ^{50}Cr was analyzed within the Skyrme quasiparticle random-phase approximation (QRPA) [26,27] and a large-scale shell model (LSSM) [8].
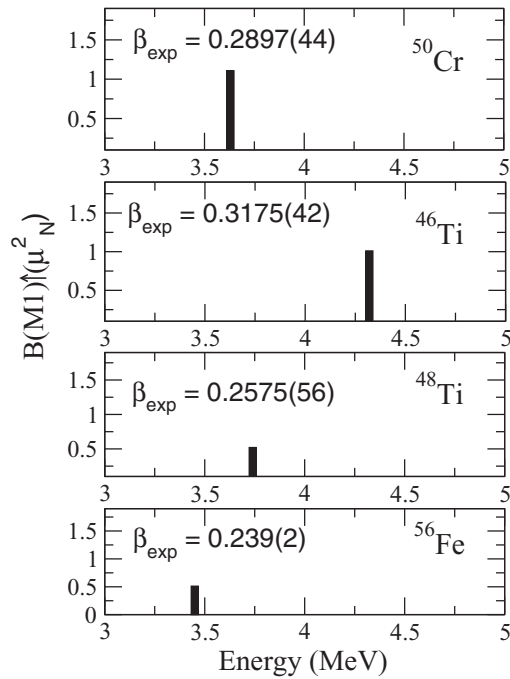
FIG. 4. $B(M1)\uparrow$ values for 1^+_{sc} states of ^{46,48}Ti [1] and ^{56}Fe [9] along with the 3.628 MeV state of ^{50}Cr. The experimental deformation parameters β_{exp} [28] are given for each nucleus.

1. Skyrme QRPA

Results of the self-consistent Skyrme-QRPA calculations are presented in Figs. 6–9 and Tables II and III. The calculations are performed with a QRPA restricted to axial symmetry [27] for axially deformed nuclei. The Skyrme QRPA method is fully self-consistent since i) both the mean field and the residual interaction are derived from the same Skyrme functional and ii) the residual interaction includes all
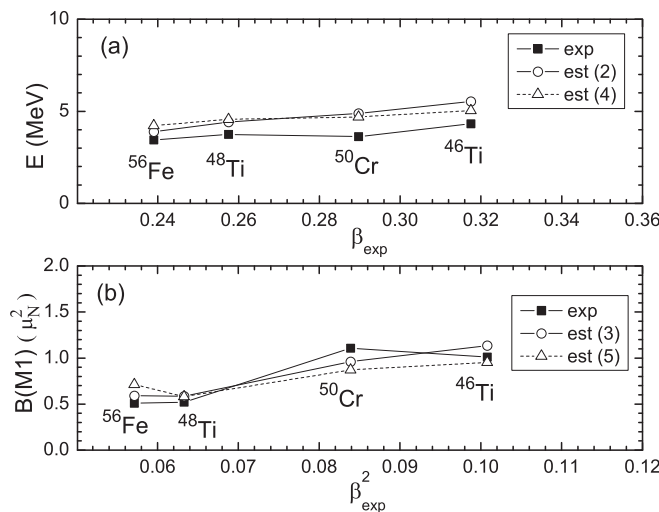

FIG. 5. Experimental 1^+_{sc} energies (top) and $B(M1)$ values (bottom) as compared to estimations (2)–(3) and (4)–(5) in ^{46,48}Ti [1], ^{50}Cr (present work), and ^{56}Fe [9]. The experimental deformation parameters β_{exp} are taken from [28].
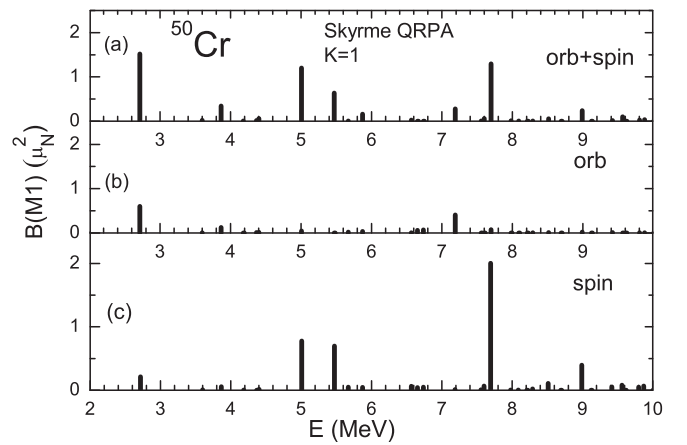

FIG. 6. Total (a), orbital (b), and spin (c) $M1$ strengths $K = 1$ calculated within Skyrme QRPA with the force SGII.

the functional contributions as well as the Coulomb direct and exchange terms. The Skyrme parametrization SGII [41] is used. The volume δ-force pairing is treated at the BCS level [44]. The parameter of the equilibrium axial quadrupole deformation $\beta = 0.30$ is determined by minimization of the total energy of the system. The calculated β is in a satisfactory agreement with the experimental value $\beta_{exp} = 0.2897(44)$ [28]. The spurious strength is concentrated below 2 MeV (not shown in Figs. 6, 7, and 9) and does not noticeably affect the results. Note that applications of the self-consistent Skyrme QRPA to magnetic orbital and spin excitations in deformed nuclei are still very limited and mainly devoted to heavy deformed nuclei, see, e.g., [42,43]. To our knowledge, the present Skyrme QRPA exploration is the first one for medium deformed nuclei.

Figure 6 presents calculated $B(M1)$ values obtained for the total (orbital + spin), orbital, and spin $M1$ transitions $I^\pi_K = 0^+_{0,\text{g.s.}} \rightarrow 1^+_{1,\nu}$ from the ground state to the νth QRPA state with $K^\pi = 1^+$. In the spin part, the familiar quenching factor of 0.7 is used. The calculations result in a 1^+ state at 2.71 MeV with a large $M1$ excitation strength of $B(M1)\uparrow =$
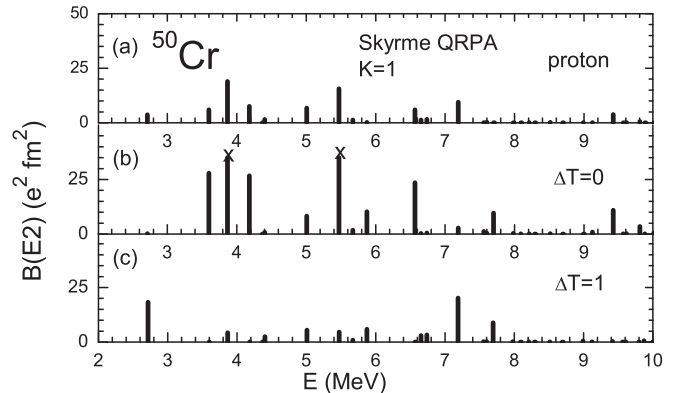

FIG. 7. Proton (a), isoscalar (b), and isovector (c) $E2$ strengths $K = 1$ calculated within the Skyrme QRPA with the force SGII. In (b), high peaks at 3.9 and 5.5 MeV [with $B(E2) = 116$ and $101 \ e^2$fm^4, respectively] are marked by crosses.
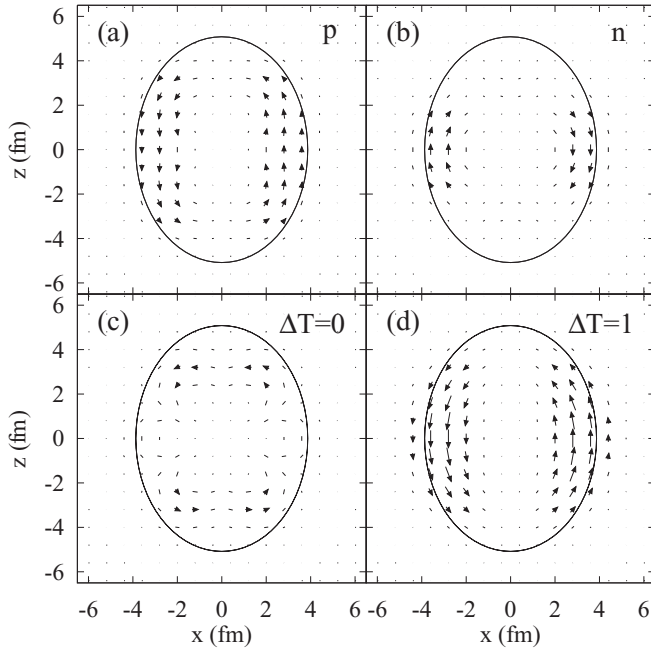
FIG. 8. Proton (a), neutron (b), isoscalar (c), and isovector (d) orbital currents in *x-z* plane for the 2.71 MeV-state calculated in the Skyrme QRPA with the force SGII. In all the panels, the currents are equally scaled to demonstrate the most strong flows. The magnitude of the current is determined by the arrow length.

TABLE II. The energies E, $B(M1)$ values and two maximal 2qp components of particular $I_{K,\nu}^{\pi}$ QRPA states with $K = 1$ and 0. The components are given in Nilsson quantum numbers $[Nn_z\Lambda]$. $\mathfrak{N}$ denotes the contribution of the component to the state norm.

E MeV	$B(M1)$ μ_N^2	p/n	2qp	$\mathfrak{N}$
		K = 1		
2.71	1.52	n	[303]7/2 [312]5/2	69%
		p	[312]5/2 [321]3/2	27%
5.01	1.20	n	[321]3/2 [321]1/2	54%
		p	[321]3/2 [321]1/2	33%
7.70	1.30	n	[312]5/2 [301]3/2	40%
		n	[321]3/2 [310]1/2	29%
		K = 0		
11.0	1.56	p	[312]5/2 [303]5/2	32%
		n	[321]3/2 [301]3/2	25%

1.52 μ_N^2. By comparing $B(M1)$ values in the plots a), b), and c), it is easy to see that the magnetic strength of this state is produced by a constructive interference of the orbital and spin parts. The orbital strength dominates which indicates a predominantly scissors-like character of the state. The mainly scissors-like nature of this state is also supported by a satisfactory agreement of its excitation energy and $B(M1)$
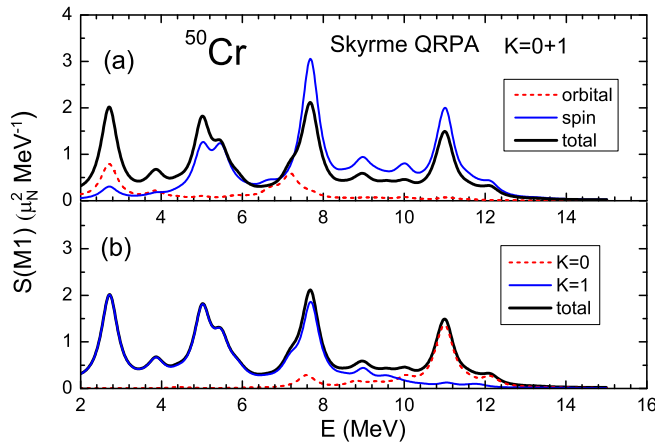
strength with the systematics for the 1_{sc}^+ as a function of nuclear deformation and mass number. Note that the calculated 2.71-MeV state is not purely orbital but has some spin admixture, which is typical [12] for light and medium deformed nuclei. Despite a noticeable energy difference, the 2.71-MeV state corresponds to the experimentally observed state at 3.628 MeV because both of them deliver experimentally and theoretically a maximal $B(M1)$ strength in the energy range 2–4 MeV.

The scissors-like character of the calculated 2.71-MeV, 1^+ state can be additionally confirmed by comparison of the proton, isoscalar ($\Delta T = 0$) and isovector ($\Delta T = 1$), $\Delta K = 1$ $B(E2; I_K^\pi = 0_{0,\text{g.s.}}^+ \rightarrow 2_{1,\nu}^+)$ values of the associated $2_{1,\nu}^+$ state belonging to the same band. These values were obtained with the effective charges $e_{\text{eff}}^p = 1, e_{\text{eff}}^n = 0$; $e_{\text{eff}}^p = e_{\text{eff}}^n = 1$; and $e_{\text{eff}}^p = -e_{\text{eff}}^n = 1$, respectively. The $B(E2)$ strengths are exhibited in Fig. 7. For the convenience of comparison with Fig. 6, the strengths are plotted as a function of the excitation energies $E_{1_{1,\nu}^+}$ for the QRPA states with $K = 1$ [The energies of $(0_{0,\text{g.s.}}^+ \rightarrow 2_{1,\nu}^+)$ transitions can be roughly estimated in the approximation that the moment of inertia of $K = 1$ bands is the same as in the ground-state band. Then the rotational

FIG. 9. Strength functions in ^{50}Cr smoothed by the Lorentz weight with $\Delta = 0.5$ MeV. (a) orbital (red dashed curve), spin (blue solid curve), and total orbital+spin (black bold curve) strengths. Contributions from all the projections ($K = 0$ and 1) are included. (b) $K = 0$ (red dashed curve), $K = 1$ (blue solid curve), and total (black bold curve) strengths.

TABLE III. Calculated $B(E2, 0_1^+ \rightarrow 2_1^+) \uparrow$ value and characteristics of the lowest $1_{1,\nu=1}^+$ state of ^{50}Cr [energy E, total excitation strength $B(M1) \uparrow$, orbital strength $B(M1)_O$, spin strength $B(M1)_S$, and ratio $R = B(M1)_O/B(M1)_S$] as compared to the present experimental data.

	Exp.	Skyrme QRPA	LSSM
$B(E2) \uparrow e^2\text{b}^2$	0.1052(32)[a]	0.11	0.108
E [MeV]	3.628	2.71	3.54
$B(M1)$ $[\mu_N^2]$	1.113(49)	1.52	0.826
$B(M1)_O$ $[\mu_N^2]$	–	0.60	0.316
$B(M1)_S$ $[\mu_N^2]$	–	0.21	0.120
R	–	2.9	2.6

[a] From Ref. [28].

increment ($E_{2^+_{1,\nu}}$-$E_{1^+_{1,\nu}}$) to $E_{1^+_{1,\nu}}$ is ∼522 keV.]. Figure 7 shows that, for the band based on the calculated 2.71-MeV state, we get a negligible $B(E2, \Delta T = 0)$ but sizeable $B(E2, \Delta T = 1)$ value. This clearly emphasizes the isovector excitation character of the state. Moreover, the $B(E2, \Delta T = 1)$ value calculated for this state is the largest for all states below 6 MeV. This observation points to the close relation of this state to the underlying quadrupole deformation. Both aspects match the isovector nature of the scissors-like mode which is usually viewed as rotation-like out-of-phase oscillations of the deformed proton and neutron subsystems.

The nature of the 2.71-MeV state is further inspected in Fig. 8, where distributions (proton, neutron, isoscalar, and isovector) of the orbital transition current of this state are exhibited. The distributions represent the proton (p) and neutron (n) transition densities of the convection current, as well as their sums ($\Delta T = 0$) and differences ($\Delta T = 1$). For the convenience of the view, the currents in all the panels are equally scaled so as to exhibit mainly the strong flows. The figure shows that the orbital motion is basically represented by rotation-like out-of-phase oscillations of protons and neutrons. Indeed in the regions of most intense flow (at the left and right nuclear surface), the protons and neutrons move in the opposite directions [compare plots a) and b)]. In these regions, the $\Delta T = 1$ motion dominates over the $\Delta T = 0$ one. It is remarkable that the $\Delta T = 1$ motion is most pronounced in the region of the nuclear equator and weak at the nuclear poles. This is surprising since the scissors-like picture suggests the opposite. One may suggest that the orbital motion in 2.71-MeV state actually corresponds not to the scissors-like flow proposed by Lo Iudice and Palumbo [13] but to an alternative picture from Lipparini and Stringari [29], where the isovector motion takes place inside the rigid surface and is maximal in the equator region. These two pictures are analogous to the Goldhaber-Teller [45] and Steinwedel-Jensen [46] treatments of the electric isovector giant dipole resonance, respectively. Our self-consistent Skyrme-QRPA results more closely correspond to the Lipparini-Stringari picture for the low-energy orbital $M1$ mode.

Now let us briefly discuss the states at $E > 4$ MeV, i.e., above the scissors-like mode. As seen from Fig. 6, these states are mainly of a spin nature with only a few exceptions at ∼4 and 6.5–7.5 MeV. The spin states form two groups at ∼5 and ∼8 MeV, that constitute altogether the $K = 1$ branch (with both $K = \pm 1$ contributions) of the $M1$ spin giant resonance.

A more general view of this resonance is given in Fig. 9 where the $M1$ strength function

$$S(M1; E) = \sum_{\nu} |\langle 1^+_{K,\nu} | \hat{M}(M1, K) | 0 \rangle|^2 \, \xi_\Delta(E - E_{1^+_{K,\nu}}) \quad (6)$$

is presented. Here, $|0\rangle$ is the ground state wave function, $|1^+_{K,\nu}\rangle$ and $E_{1^+_{K,\nu}}$ are QRPA states and energies, $\hat{M}(M1, K)$ is the $M1$ transition operator with the projection K, $\xi_\Delta(E - E_{1^+_{K,\nu}}) = \Delta/(2\pi[(E - E_{1^+_{K,\nu}})^2 - \Delta^2/4]$ is the Lorentz smoothing with the averaging parameter $\Delta = 0.5$ MeV.

Figure 9 shows that the spin resonance basically consists of two bumps at ∼5 and ∼8 MeV from the $K = 1$ branch and the bump at ∼11 MeV from the branch $K = 0$. Altogether
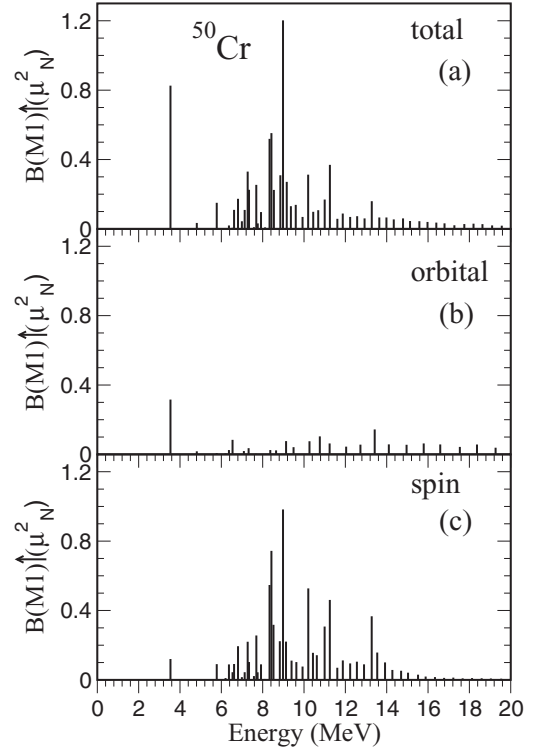

FIG. 10. Total (a), orbital (b), and spin (c) $M1$ excitation strengths calculated within a large-scale shell-model with the KB3G interaction.

spin excitations fill a broad region from 5–13 MeV, which well matches a resonance region in LSSM calculations, see Fig. 10 below. In our QRPA calculations, the spin resonance is not concentrated in one broad bump but looks like a sequence of few well separated structures. This may be expected from the fact that QRPA omits parts of the spin correlations. As seen from Fig. 10, the inclusion of more correlations in the LSSM allows to mix the separate structures and to form a broad regular resonance.

Figure 9(a) shows that the interference of the orbital and spin excitations is constructive at $E < 7$ MeV and destructive at higher energies. As seen from Fig. 9(b), the excitations in the energy interval of our interest, $E < 10$ MeV, almost completely belong to the $K = 1$ branch. In the energy interval 4.5–14 MeV where the spin $M1$ resonance is localized, the calculated total $M1$ strength is ∼5.9 μ^2_N. This is in accordance with the experimental strengths of 5–7 μ^2_N found in ^{24}Mg and ^{28}Si [2]. For the interval 2–9.7 MeV covered by the present experiment, the calculations give a total strength of ∼6.2 μ^2_N which somewhat overestimates the total observed $M1$ strength ∼4.01 μ^2_N.

It is instructive to see the structure of the QRPA states providing the dominant contribution to the orbital and spin bumps in Fig. 9. This information is given in Table II. The table shows that the calculated 1^+_{sc} at 2.71 MeV is formed by $\Delta K = 1$ transitions between the levels [303]7/2, [312]5/2, and [321]3/2. They are neighboring levels arising due to the deformation splitting of the $1f_{7/2}$ subshell. Thus one encounters here a typical scheme for orbital excitations. Note

that the collectivity of the 2.71-MeV state is low. Its two largest components exhaust 96% of the norm.

Table II also shows the structure of the calculated states at 5.01, 7.70, and 11.0 MeV that strongly contribute to the main parts of the spin $M1$ resonance in Fig. 9. It is seen that these states are rather collective. Their two largest components give altogether only 57–87 % of the norm. Some of the components, e.g., [312]5/2-[301]3/2 in the 7.70 MeV-state and [321]3/2-[301]3/2, [312]5/2-[303]5/2 in the 11.0 MeV-state directly correspond to the $1f_{7/2} - 1f_{5/2}$ spin-flip transition. The strong deformation splitting spreads the strength of $1f_{7/2} - 1f_{5/2}$ transitions over different QRPA states. Since the QRPA description does not include all correlations, the spin $M1$ resonance is yet represented by a small number of states and looks like a sequence of a few separated structures. The more comprehensive picture of the spin $M1$ resonance is given below in terms of the shell model which includes more correlations.

2. Large-scale shell model

The results of the LSSM calculations are presented in Fig. 10. We start with a reminder of the computational procedures used in [37], which we follow here. In the spherical shell model, ^{50}Cr is described in a $0\hbar\omega$ space, i.e., ten particles are allowed to occupy all the states available in the fp shell. The KB3G [47] interaction is used. The single-particle energies are taken from the experimental spectrum of ^{41}Ca.

Figure 10 shows $B(M1)$ values obtained for the total (orbital + spin), orbital, and spin $M1$ transitions. In the spin part, a quenching factor of 0.75 [48] is used. The calculations give the state at 3.5 MeV with a sizable strength $B(M1) = 0.826 \ \mu_N^2$. The orbital strength dominates the 3.5 MeV state, which indicates the scissors-like character of the state. It should be pointed out that in the LSSM the 3.5-MeV state is not purely orbital but also has some spin admixture, which appears in the QRPA calculations. The calculated 3.5-MeV state matches remarkably well with the experimentally observed state at 3628.2 keV.

The LSSM calculations show that $M1$ transitions above 3.6 MeV are mainly of spin character (see lower panel of Fig. 10). The calculated summed $M1$ strength in the experimentally investigated energy range from 2–9.7 MeV amounts to ~5.6 μ_N^2 as compared to the measured value of 4.1(1) μ_N^2. The total calculated strength in the resonance, energy interval 4.5–14 MeV, is ~6.6 μ_N^2 in good correspondence to the QRPA result of 5.9 μ_N^2.

In Table III, the LSSM results are compared to QRPA ones and present experimental data. The table shows that the LSSM better describes the level energy than the Skyrme QRPA. Most probably this is because the LSSM takes into account the coupling to complex configurations, omitted in the QRPA.

IV. SUMMARY AND OUTLOOK

The low-lying $M1$-strength in the open-shell nucleus ^{50}Cr has been determined with the method of nuclear resonance fluorescence using bremsstrahlung at the superconducting Darmstadt linear electron accelerator S-DALINAC and Compton backscattered photons at the High Intensity γ-ray Source (HIγS) facility. Fifteen 1^+ states have been observed between 3.6 and 9.7 MeV. Further, 14 γ-ray transitions and 13 $B(M1)$ values have been measured for the first time.

The experimental results were compared to calculations in the self-consistent Skyrme quasiparticle random-phase approximation (QRPA) [26] and the large-scale shell model (LSSM) [8]. The QRPA allowed to highlight the basic features and origin of 1^+ states while the LSSM demonstrated the important role of complex configurations. Both models reproduce the similar $B(E2)$ values.

Following our theoretical analysis and comparison with other available results for fp-shell nuclei the lowest 1^+ state at 3.6 MeV was identified as an isovector orbital mode with some spin admixture. In agreement with previous studies for fp-shell nuclei [9], a constructive interference of the orbital and spin contributions for this state was confirmed. This augments the previous rare data (^{46,48}Ti [1] and ^{56}Fe [9]) on this orbital mode in the fp-shell region. The obtained data match the estimations and trends for the scissors-like mode in a satisfactory way.

It is also interesting that distributions of the orbital current, computed within the Skyrme QRPA for the lowest 1^+ state, favor the schematic picture of Lipparini and Stringari [29] (isovector rotation-like oscillations inside the rigid surface) rather than the scissors-like view of Lo Iudice and Palumbo [13].

The spin excitations above the scissors-like mode were also inspected. The QRPA calculation confirms that the spin $M1$ resonance in ^{50}Cr is provided by spin-flip transitions (mainly $1f_{7/2} - 1f_{5/2}$) inside the fp shell.

ACKNOWLEDGMENTS

[1] A. Richter, Nucl. Phys. A **507**, 99 (1990).

[2] M. N. Harakeh and A. van der Woude, *Giant Resonances* (Oxford University Press, Oxford, 2001).

[3] D. Zawischa, J. Phys. G **24**, 683 (1998).

[4] P. von Brentano *et al.*, Prog. Part. Nucl. Phys. **46**, 197 (2001).

[5] N. Pietralla, P. von Brentano, and A. F. Lisetskiy, Prog. Part. Nucl. Phys. **60**, 225 (2008).

[6] K. Heyde, P. von Neumann Cosel, and A. Richter, Rev. Mod. Phys. **82**, 2365 (2010).

[7] I. Talmi, Adv. Nucl. Phys. **27**, 1 (2003).

[8] E. Caurier, G. Martinez-Pinedo, F. Nowacki, A. Poves, and A. P. Zuker, Rev. Mod. Phys. **77**, 427 (2005).

[9] R. W. Fearick *et al.*, Nucl. Phys. A **727**, 41 (2003).

[10] K. Hara, T. Adachi, H. Akimune, I. Daito, H. Fujimura, Y. Fujita, M. Fujiwara, K. Fushimi, K. Y. Hara, M. N. Harakeh, K. Ichihara, T. Ishikawa, J. Janecke, J. Kamiya, T. Kawabata, K. Kawase, K. Nakanishi, Y. Sakemi, Y. Shimbara, Y. Shimizu, M. Uchida, H. P. Yoshida, M. Yosoi, and R. G. T. Zegers, Phys. Rev. C **68**, 064612 (2003).

[11] Y. Fujita *et al.*, J. Phys. G **35**, 014041 (2008).

[12] A. F. Lisetskiy *et al.*, Nucl. Phys. A **677**, 100 (2000).

[13] N. Lo Iudice and F. Palumbo, Phys. Rev. Lett. **41**, 1532 (1978).

[14] F. Iachello, Nucl. Phys. A **358**, 89 (1981).

[15] D. Bohle *et al.*, Phys. Lett. B **137**, 27 (1984).

[16] N. Lo Iudice, Phys. Elem. Part. Atom. Nucl. **28**, 1389 (1997).

[17] A. Willis *et al.*, Nucl. Phys. A **499**, 367 (1989).

[18] J. Enders *et al.*, Nucl. Phys. A **636**, 139 (1998).

[19] R. Moreh *et al.*, Phys. Rev. C **2**, 1144 (1970).

[20] U. Kneissl, H. H. Pitz, and A. Zilges, Prog. Part. Nucl. Phys. **37**, 349 (1996).

[21] U. Kneissl, N. Pietralla, and A. Zilges, J. Phys. G **32**, R217 (2006).

[22] F. R. Metzger, Prog. Nucl. Phys. **7**, 54 (1959).

[23] A. Richter, in *Proceedings of the 5th European Particle Accelerator Conference, Barcelona* (Institute of Physics, Bristol/Philadelphia, 1996), p. 110.

[24] K. Sonnabend *et al.*, Nucl. Instrum. Methods Phys. Res. A **640**, 6 (2011).

[25] H. R. Weller *et al.*, Prog. Part. Nucl. Phys. **62**, 257 (2009).

[26] P. Ring and P. Schuck, *Nuclear Many Body Problem* (Springer-Verlag, New York, 1980).

[27] A. Repko, J. Kvasil, V. O. Nesterenko, and P.-G. Reinhard, arXiv:1510.01248 [nucl-th].

[28] B. Pritychenko, M. Birch, B. Singh, and M. Horoi, At. Data Nucl. Data Tables **107**, 1 (2016).

[29] E. Lipparini and S. Stringari, Phys. Lett. B **130**, 139 (1983).

[30] S. Agostinelli *et al.*, Nucl. Instrum. Methods Phys. Res. A **506**, 250 (2003).

[31] N. Pietralla *et al.*, Nucl. Instrum. Methods Phys. Res. A **483**, 556 (2002).

[32] N. Pietralla, Z. Berant, V. N. Litvinenko, S. Hartman, F. F. Mikhailov, I. V. Pinayev, G. Swift, M. W. Ahmed, J. H. Kelley, S. O. Nelson, R. Prior, K. Sabourov, A. P. Tonchev, and H. R. Weller, Phys. Rev. Lett. **88**, 012502 (2001).

[33] H. Stein, Diploma thesis, Institut für Kernphysik, Darmstadt, 1988 (unpublished).

[34] Z. Elekes, J. Timar, and B. Singh, Nucl. Data Sheets **112**, 1 (2011).

[35] H. Pai, J. Beller, N. Benouaret, J. Enders, T. Hartmann, O. Karg, P. vonNeumann-Cosel, N. Pietralla, V. Y. Ponomarev, C. Romig, M. Scheck, L. Schnorrenberger, S. Volz, and M. Zweidinger, Phys. Rev. C **88**, 054316 (2013).

[36] G. Alaga, Phys. Rev. **100**, 432 (1955).

[37] G. Martinez-Pinedo, A. Poves, L. M. Robledo, E. Caurier, F. Nowacki, J. Retamosa, and A. Zuker, Phys. Rev. C **54**, R2150(R) (1996).

[38] N. Lo Iudice and A. Richter, Phys. Lett. B **304**, 193 (1993).

[39] N. Pietralla, P. von Brentano, R.-D. Herzberg, U. Kneissl, N. Lo Iudice, H. Maser, H. H. Pitz, and A. Zilges, Phys. Rev. C **58**, 184 (1998).

[40] S. Raman, C. W. Nestor, Jr., and P. Tikkanen, At. Data Nucl. Data Tables **78**, 1 (2001).

[41] N. Van Giai and H. Sagawa, Phys. Lett. B **106**, 379 (1981).

[42] P. Vesely, J. Kvasil, V. O. Nesterenko, W. Kleinig, P.-G. Reinhard, and V. Yu. Ponomarev, Phys. Rev. C **80**, 031302(R) (2009).

[43] V. O. Nesterenko, J. Kvasil, P. Vesely, W. Kleinig, and P.-G. Reinhard, Int. J. Mod. Phys. E **19**, 558 (2010).

[44] M. Bender, K. Rutz, P.-G. Reinhard, and J. A. Maruhnm, Eur. Phys. J. A **8**, 59 (2000).

[45] M. Goldhaber and E. Teller, Phys. Rev. **74**, 1046 (1948).

[46] H. Steinwedel and J. H. D. Jensen, Z. Naturforsch. **5a**, 413 (1950).

[47] A. Poves *et al.*, Nucl. Phys. A **694**, 157 (2001).

[48] P. von Neumann-Cosel *et al.*, Phys. Lett. B **443**, 1 (1998).